energies

MDPI

Article

Sustainability and Cost Effectiveness Analysis of Staggered Jet Impingement on Solar Thermal Collector

Rajesh Maithani [1], Anil Kumar [1,*], Manoj Kumar [2,*] and Sachin Sharma [1,*]

[1] Department of Mechanical Engineering, University of Petroleum and Energy Studied, Dehradun 248007, India
[2] Department of Mechanical Engineering, DIT University, Dehradun 248009, India
* Correspondence: k.anil@ddn.upes.ac.in (A.K.); drmanoj.kumar@dituniversity.edu.in (M.K.); sachin.sharma@ddn.upes.ac.in (S.S.)

Abstract: The sustainability index, waste energy ratio and improvement potential of a staggered air jet impingement on the staggered spherical protrusions of a roughened absorber plate were derived for the present study to evaluate exergy losses and irreversibility in the system. The experimental analysis was carried out for selected parameters: relative streamwise pitch, relative spanwise pitch and relative jet diameter to hydraulic diameter ratio. The flow Reynolds number ranged from 4000–18,000. The augmentation in Nusselt number and friction factor compared to a smooth surface was 4.9 and 12.4 times, respectively. The statistical correlation developed determined the maximum thermohydraulic performance parameter and exergetic efficiency be 3.02 and 3.87%, respectively. The magnitude of the sustainability index, waste energy ratio and improvement potential was found to be 1.0347, 0.962 and 10.84, respectively, for the entire range of tested parameters. A cost analysis was also performed to evaluate the cost-effectiveness of the solar thermal system with and without turbulent promoters.

Keywords: jet impingement; protrusion roughness; sustainability index; waste heat recovery

Citation: Maithani, R.; Kumar, A.; Kumar, M.; Sharma, S. Sustainability and Cost Effectiveness Analysis of Staggered Jet Impingement on Solar Thermal Collector. *Energies* **2022**, *15*, 7345. https://doi.org/10.3390/en15197345

Academic Editor: Andrea De Pascale

Received: 9 September 2022
Accepted: 4 October 2022
Published: 6 October 2022

1. Introduction

Increasing renewable energy demands are leading to the enhancement of the performance of solar thermal systems, which are applied in various domains [1]. A lower thermal efficiency in terms of the solar thermal collector (*STC*) due to an inferior convective heat transfer coefficient is a major obstacle to harvesting thermal energy. The deficiency can be overcome by unsettling the boundary layer formed on the heat transfer surface by creating artificial roughness of different forms such as transverse and angled ribs, V, W and Z-shaped ribs, a dimple and protrusion-shaped roughness, baffles and blockages [2]. The impinging jet is reported to be an effective method for heat transfer enhancement [3]. The integration of an artificially roughened heated plate with the impinging of air to enhance the convective heat transfer coefficient [4,5] is an effective technique when used to harvest good amount of thermal energy. A lower thermal efficiency in terms of the solar thermal collector (*STC*) due to inferior convective heat transfer coefficient is a major obstacle to harvesting thermal energy.

Nadda et al. [6] analyzed a heated surface roughened with a protrusion in an arc shape by impinging the air jets on a solar air heater (SAH) absorber plate. A maximum thermal hydrodynamic performance of 1.5 was achieved. Kercher and Tabakoff [7] analyzed streamwise and spanwise pitches in a low velocity jet impingement process. Nadda et al. [8] analyzed an SAH duct for thermal performance by impinging air jets on the heated absorber plate. The investigation reported that the heat transfer enhancement was significant, but the corresponding pressure drop penalty decreased the overall thermohydraulic performance of the SAH, as determined by the preference selection index (*PSI*) methodology. Metzger et al. [9] studied the effect of the staggered impingement of air jets on a heated

surface. The results reported that the incorporation of jets in staggered arrangements are not better than the in-line arrangement of jets in terms of thermal performance for the selected parameters. Chauhan et al. [10] analyzed the effect of employing the air jets impinging on a heated absorber plate surface with an aim of analyzing the thermal performance of the SAH duct. The various geometric parameters considered were the pitches in the flow direction and transverse direction, the diameter of the jet and the flow (Re). The outcome of the analysis revealed a substantial improvement in the Nu ratio of 2.67. Brevet et al. [11] investigated the array of air jet impinging on a heated surface for a range of jet impingement distances and spanwise jet-to-jet spacing. The air leaving the heated section after impingement was directed in a particular direction. The analysis resulted in the determination of the parametric values for spanwise jet-to-jet spacing and impingement distance to be 3 to 6 and 4 to 5, respectively. Nadda et al. [12] experimentally analyzed an SAH duct for its heat transfer and friction characteristics by impinging circular air jets on the heated surface. The analysis was carried out by selecting various geometric parameters, i.e., relative height ratio, relative width ratio, relative pitch ratio and the angle of the arc. The Nu and f ratios, when compared with the smooth duct of an SAH, were found to be 6.29 and 9.25, respectively, and the extreme thermohydraulic performance parameter achieved was 3.64. Mishra et al. [13] experimentally studied the effect of various parameters on a solar air passage with air jet impingement. An analytical hierarchy preference selection process using the (AHP-TOPSIS) technique was used to determine the set of geometric parameters that deliver the highest thermal performance with minimum friction losses. Sedighi et al. [14] analyzed the cooling effect by impinging four air jets in a turbulent regime on a heated plate with the parameters selected as follows: the distance between the jets and the heated plate, the distance between the jets, the angle of the jets and the distance between the outer and inner jets. The results reported that the Nu is enhanced when the impinging jet angles are fixed at a higher Re, when the jet-to-jet and jet-to-heated surface spaces are smaller and when there is a broader opening in terms of the outer jets. The swirling air jet impinging on the heated SAH absorber plate was analysed numerically by Afroz and Sharif [15], who reported an 8% enhancement in the Nu by incorporating a swirling motion, as compared to a non-swirling motion.

The analysis of thermal performance using jet impingement is supported by the numerical techniques of various investigators. Issac et al. [16] experimentally and numerically analyzed the performance of a round jet for various nozzle to plate spacing. The numerical analysis was carried out using a different RANS turbulence model. The results reported that the magnitudes of the inlet turbulent intensity and eddy viscosity play a major role in performance enhancement. N. Celik [17] applied the design of experiment (DoE) and analysis of variance ($ANOVA$) to an experimental investigation of impinging jets. The major factors considered for investigation were the roughness of the heated surface and the jet geometry. It was reported that the Nu highly was affected by the radial distance, whereas the effect in terms of surface roughness was much lower. Singh et al. [18] examined the influence of air jet impinging on a rectangular duct of double pass SAH with a corrugated wavy shape jet plate. A bed porosity of 98% and impinging plate perforation of 0.48% yielded a maximum thermal efficiency of 94%. Kumar et al. [19] investigated an SAH duct with air jet impinging through a circular inside conical ring and found that the maximum thermos-hydraulic performance parameter was 2.16. Different configuration in terms of inner conical ring obstacles were analyzed by Kumar et al. [20] using an SAH rectangular duct with impinging air jets and an of Re from 5000 to 23,000. The maximum rate of heat transfer obtained was of the order of 2.33. Statistical correlations using the regression analysis were developed for Nu and f. Erasmus et al. [21] experimentally and numerically investigated the impinging of an air jet on a concave hemispherical surface using computational tools. The correlation in terms of Nusselt number and the total pressure loss was developed in terms of Reynolds number and the Prandtl number.

The above literature study reveals that impinging jets are a significant heat enhancement technique. Artificial roughness generates a secondary flow because of the generation

of vortices, which enhances the convective heat transfer. A staggered fluid jet impinging on the heated surface with a staggered roughness will boost the heat transfer, and it was this objective that the present study investigated. The parameters selected for investigation are novel, as there is no literature review present for the analysis of staggered jets on a staggered spherical protrusion location. The jets were impinging on the heated surface at the location where the surface was roughened in form of spherical protrusions. The location of the jet was exactly below the hemispherical protrusions, and the jet and protrusion diameters were the same. The location of the perpendicular striking staggered jets was exactly below the spherical protrusions to diverge the span of the jet to a larger area. A schematic of the jet position on the plate and the protruded plate is shown in Figure 1. The range of flow and geometrical parameters selected for the experimental investigation were: The relative jet diameter to hydraulic diameter ratio (d_j/D_h) ranged from 0.043–0.086, the relative streamwise pitch (X/D_h) was in the range of 0.869–2.173 and the relative spanwise pitch (Y/D_h) was in the range of 0.434–1.08; the flow Reynolds number (Re) was selected in the range of 4000–18,000.

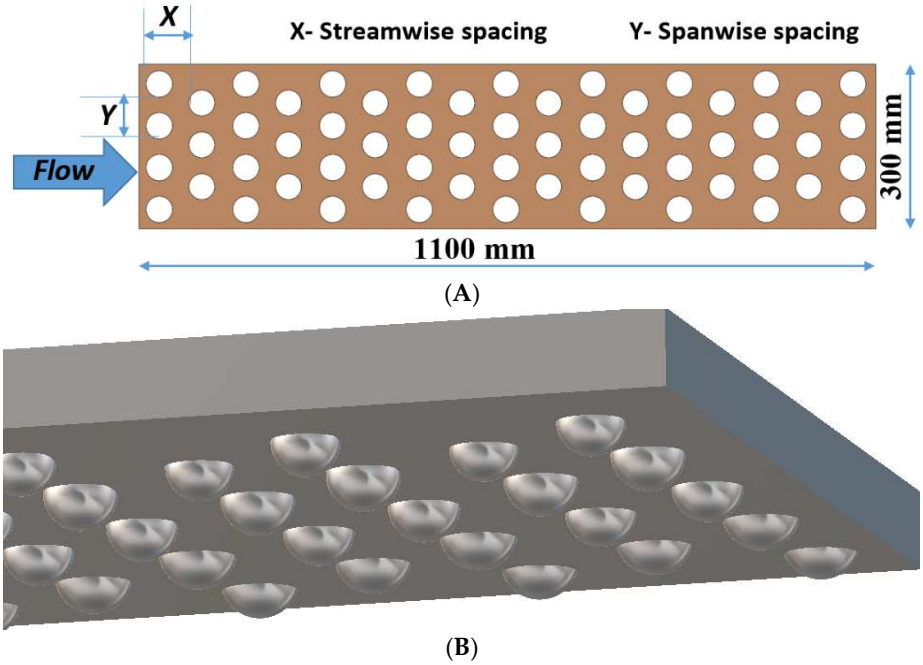

Figure 1. (**A**) Jet position on plate and (**B**) test plate with staggered protrusions.

The methodology followed in the present investigation is displayed in Figure 2. The process of data collection was followed by thermos-hydraulic performance analysis, correlation development, exergy calculation, a sustainability assessment and finally a cot analysis of the thermal system.

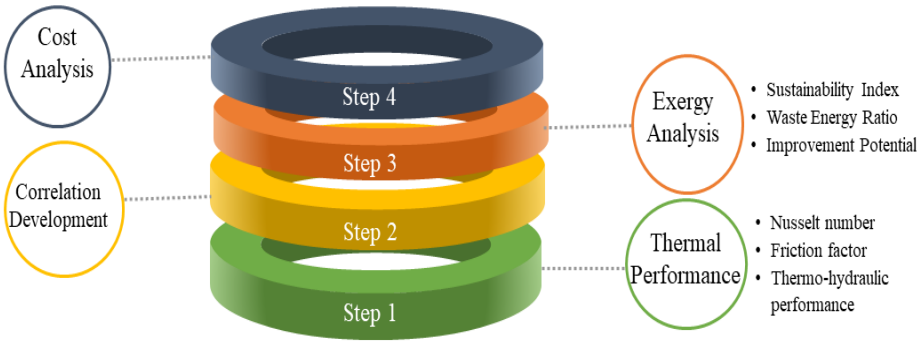

Figure 2. Methodology of the present investigation.

2. Experimental Facility

The experimental test rig (Figure 3) consisted of test, entry and exit section lengths of 1.1, 0.43 and 0.21 m, respectively, according to the ASHRAE standards [22]. A heat flux of 1000 W/m^2 was simulated indoors with the help of a nichrome wire electric heater controlled by a variable transformer. The transformer parameters were controlled by a voltmeter and ammeter with a count of at least 1 V and 0.01 A, respectively. The flow Reynolds number through the test section was determined with the aid of a U-tube manometer with a count of at least 1 mm, and the pressure drop penalty across the investigated heated section was measured by an at least 0.1 Pa count digital micro-manometer. The working fluid temperature was measured at the inlet and outlet of the test section and the heated surface by 21 calibrated (PRESYS T-25N Calibrator, least count 0.01 °C) J-Type thermocouples with an accuracy of ±0.1 °C. Air was circulated through the test section by a 2 HP centrifugal blower. The perforated impingement jet plate was inserted between the heated test plate and the bottom surface of the rectangular duct.

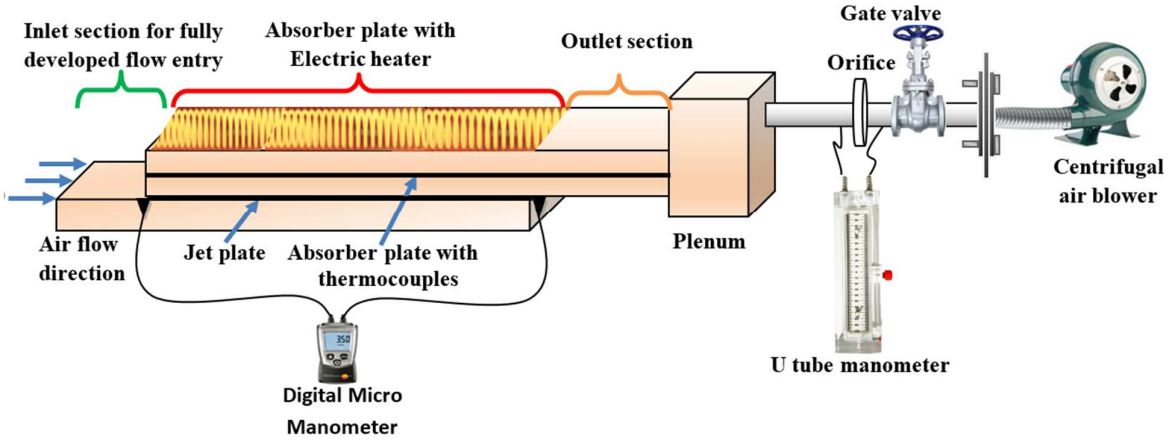

Figure 3. Schematic of experimental test facility.

3. Data Reduction

The temperature and pressure drop data collected experimentally is presented in the dimensionless form as Nusselt number (Nu) and friction factor (f), respectively. The computation starts with the calculation of the air mass flow rate ($\dot{m}$) from the pressure drop (ΔP_o) determined by the calibrated orifice plate with area of A_o. Air is the cooling medium in the rectangular channel, with physical properties (μ_a, $c_{p,a}$, k_a) calculated on the basis of the temperature of the air at the experimental location. The $\dot{m}$ is determined using the following formula.

$$\dot{m} = C_d A_o \left[2\rho \Delta P_o / \left(1 - \beta^4\right)\right]^{0.5} \quad (1)$$

where $\Delta P_o = 9.81 \Delta h_o \rho_m$ and C_d is the coefficient of discharge.

The flow Reynolds number (Re) through the setup of the hydraulic diameter (D_h) is found by:

$$Re = \rho_a V D_h / \upsilon_a \quad (2)$$

The pressure drop (ΔP_d) generated across the duct determines the friction factor (f) by applying the Darcy equation as

$$f = 2(\Delta P_d) D_h / 4 \rho_a L V^2 \quad (3)$$

The heat transfer coefficient (h) of the heated plate is used to determine the Nusselt number (Nu)

$$Nu = h D_h / K \quad (4)$$

Using the uncertainty method proposed by Kline [23], the highest uncertainties in terms of the mass flow rate: ±2%, Reynolds number: ±2.5%, Nusselt number: ±4.9% and friction factor: ±4.7% was determined.

4. Cost Analysis

A cost study was carried out in order to calculate the solar air heater's cost to benefit ratio (CTBR). The CTBR compares the solar air heater's annual costs (AC) per unit surface area to the solar air heater's energy gained annually (EGA) [24,25].

$$CTBR = \frac{AC}{EGA} \tag{5}$$

Collector annual cost (CAY), pumping annual cost (PAC), annual maintenance cost (AMC) and annual salvage value (ASV) are all included in the $AC(ASV)$. These variables are connected to annual costs in the following way:

$$AC = CAY + PAC + AMC - ASV \tag{6}$$

$$CAY = IC \times CRF \tag{7}$$

$$IC = CCA + SFC + TFC \tag{8}$$

where IC is the initial cost.

The Capital reclamation factor is

$$CRF = \frac{i(i+1)^t}{(i+1)^t - 1} \tag{9}$$

where i = annual interest rate, t = the lifetime of the collector

$$PAC = \dot{m}_a \times (\Delta \mathrm{P})_\mathrm{d} / \rho_a \times OT \times EC \tag{10}$$

OT = operation time and EC = electricity cost.

$$AMC = 0.1 \times IC \tag{11}$$

$$ASV = SV \times SFF \tag{12}$$

The salvage value (SV) is given as

$$SV = 0.01 \times IC \tag{13}$$

and the sinking fund factor (SFF) is defined as

$$SFF = \frac{i}{(i+1)^t - 1} \tag{14}$$

$$EGA = \dot{m}_a c_p (T_o - T_i) \times OT \tag{15}$$

5. Validity Test

The validity of the experimental data in terms of Nu was tested using the Dittus–Boelter equation (Equation (16)) and the Gnielinski equation (Equation (17)) and for the Nu represented as for a smooth duct.

$$Nu = 0.023 Re^{0.8} Pr^{0.4} \tag{16}$$

The Gnielinski equation for the Nusselt Number for $2300 < Re < 5 \times 10^6$ is:

$$Nu = \frac{\left(\frac{f}{2}\right)(Re - 1000)Pr}{1 + 12.7\left(\frac{f}{2}\right)^{\frac{1}{2}}\left(Pr^{\frac{2}{3}} - 1\right)} \quad (17)$$

where $f = \left(1.58\ in\ Re^{-3.82}\right)^{-2}$.

The friction factor (f) was validated using the standard Petukhov equation (Equation (18)) and modified Blasius equation (Equation (19)) for a smooth duct surface of a SAH and is given as:

The Petukov equation for the friction Factor for $3000 < Re < 5 \times 106$ is:

$$f = \left(0.79\ lnRe^{-1.64}\right)^{-2} \quad (18)$$

and the modified Blasius equation is:

$$f = 0.085Re^{-0.25} \quad (19)$$

Figure 4 shows the experimental and predicted Nu and f values. The average deviation of the Nu was ±7.4% while that of the f was ±8.3%.

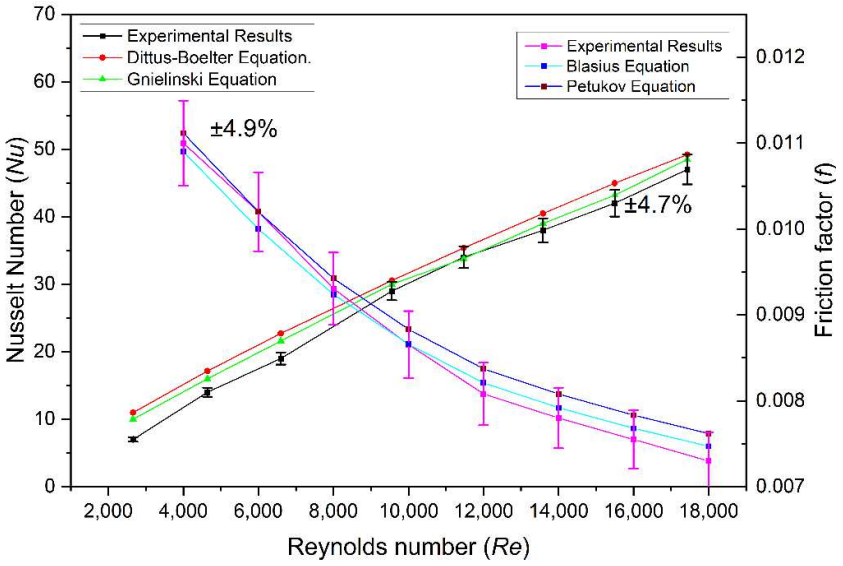

Figure 4. Experimental and predicted values for Nu and f .

6. Results and Discussion

Figure 5 shows the variations in the Nu with Re for different ranges of d_j/D_h with a constant X/D_h of 1.739 and Y/D_h of 1.08. The Nu increases with an increase in Re and its values are highest for a d_j/D_h of 0.086. As the d_j/D_h increases, the air flow through the staggered jet increases, which affects more of the heated surface by jet impingement, and this increased flow of air leads to heat transfer augmentation. The intensity with which the air jet impinges on the heated surface increases until a ratio of 0.086, beyond which the turbulent intensity of jet impinging on the surface decreases due to the higher diameter of the jet and thus the lower intensity of turbulence caused by a higher mass air flow rate, with a low striking velocity causing a downfall in the heat transfer rate. The Nu data for a range of Re in terms of roughened ducts at different relative streamwise pitches (X/D_h) for a relative spanwise pitch (Y/D_h) of 1.08 and a relative jet diameter to hydraulic diameter ratio (d_j/D_h) of 0.086 is shown in Figure 6. The introduction of a protrusion on the absorber plate allows for an increment in heat transfer. As the air mass flow and the number of air impinging jets increases on the heated absorber plate, the heat transfer increases by

raising the value of parameter X/D_h. The highest Nu was obtained at an X/D_h of 1.739, and beyond this the Nu decreased because the number of rows in a streamwise direction decreased, which leads to lower reattachment points.

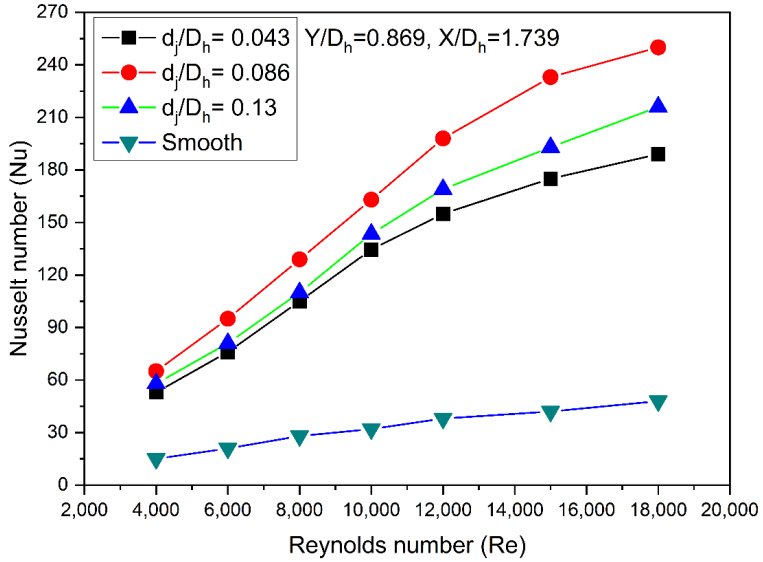

Figure 5. Shows variation in Nu with Re for different ranges of d_j/D_h.

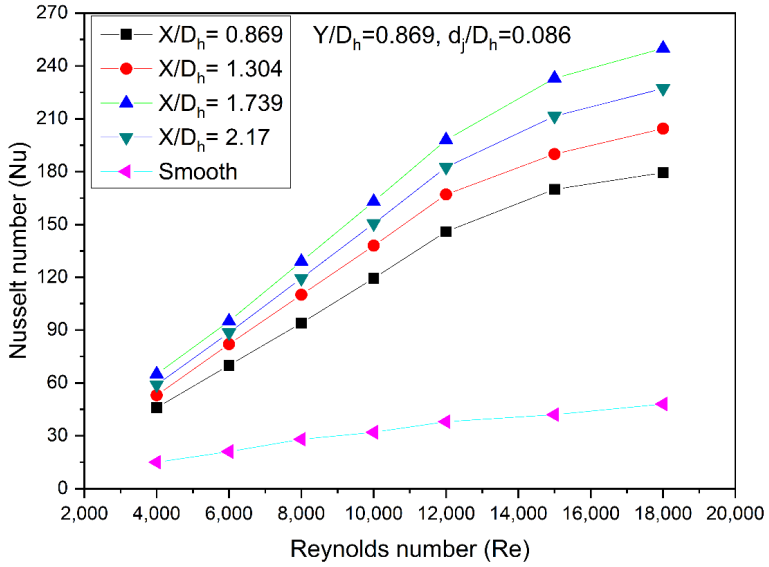

Figure 6. Shows variation in Nu with Re for different ranges of X/D_h.

The air jet impinging on the spherical protrusion surface is seen in Figure 7. The air jet striking the spherical protrusion spreads over the protruded surface as well as the flat heated surface and disrupts the larger laminar sub-layer, thus eliminating larger hot zone areas, which leads to augmented heat transfer. Figure 8 reveals the effect of Y/D_h on Nu at various Re values for an X/D_h of 1.739 and a d_j/D_h of 0.086. It is seen that the Nu continuously rises with an escalation in the Y/D_h up to a value of 1.08, with the Nu subsequently decreasing. The probable reason for this enhancement is that as the spanwise spacing increases, it provides an area for the jet stream to spread-out on and merge with neighboring jet streams. This amalgamation of the jet streams enhances the turbulence and hence the heat transfer is improved. Whereas an increase in Y/D_h beyond 1.08 results in larger area between air jet streams, the intensity with which they interact with the neighboring jet stream is lower. Thus, it can be concluded that the Y/D_h plays

an important role in enhancing the Nu by impinging the spanwise air to eliminate larger hot zones.

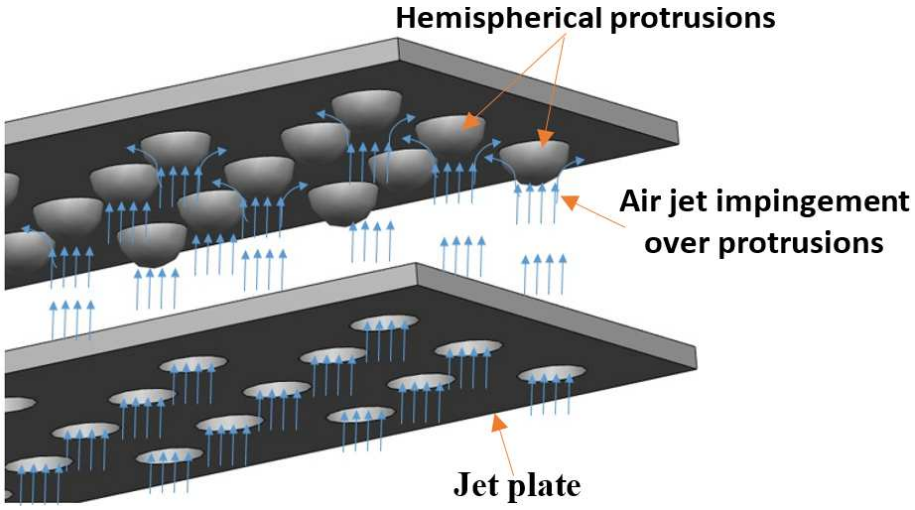

Figure 7. Air jet impinging flow pattern on protrusions.

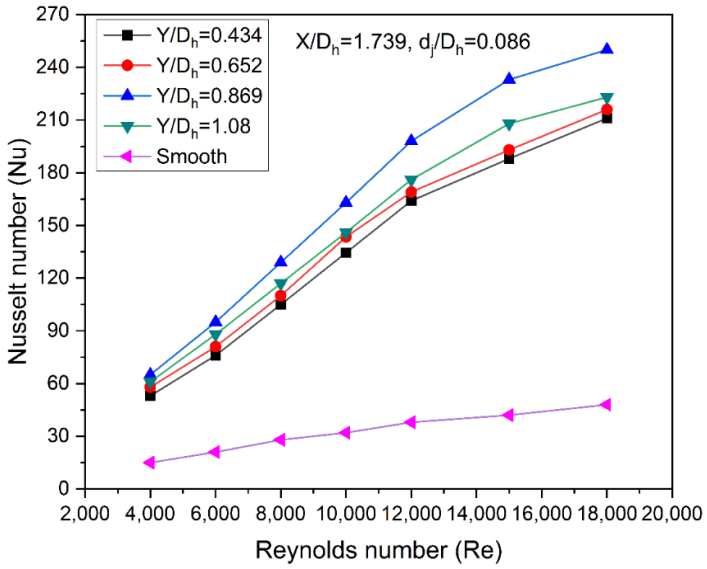

Figure 8. Shows variation in Nu with Re for different ranges of Y/D_h.

Figure 9 shows the effect of d_j/D_h on f at various Re values for fixed X/D_h value of 1.739 and a Y/D_h value of 1.08. The results show that the f for a d_j/D_h of 0.043 is in the maximum range of Re values investigated. As the size jet holes increase from a d_j/D_h ratio of 0.043 to one of 0.130, more air should be pass through it, which results in a lower f. The variation in f with Re for various X/D_h values is shown in Figure 10 for a Y/D_h of 1.08 and a d_j/D_h of 0.086. It is seen that the value of f goes down with an increasing Re. The protrusion-facing surface experiences higher values of f than that of the smooth duct. Since the pressure drop increases because of the presence of protrusions, a secondary flow is generated on either side of the protrusion ducts. Any increase in the X/D_h value beyond 1.739 reduces the value of f, as number of jets striking the heated plate reduces, which leads to a lower intensity in terms of the turbulence. The plots show that the maximum f for the duct occur in the case of an X/D_h of 1.739. Strength and intensity of secondary flow deteriorated in case of an X/D_h of 0.869, as compared to an X/D_h of 1.739 and 2.173; hence, the f is lower in such cases. The variation in f with an Re of a roughened duct at different Y/D_h values, while keeping the other parameters values constant, is displayed in Figure 11, with corresponding values for the smooth duct. The f value decreases with an

increase in Re. As the Y/D_h value changes from 0.434 to 1.08, the number of jets impinging on the heated plate reduces, which leads to smaller area for air transfer, which in turn lowers the intensity of turbulence and causes a higher f.

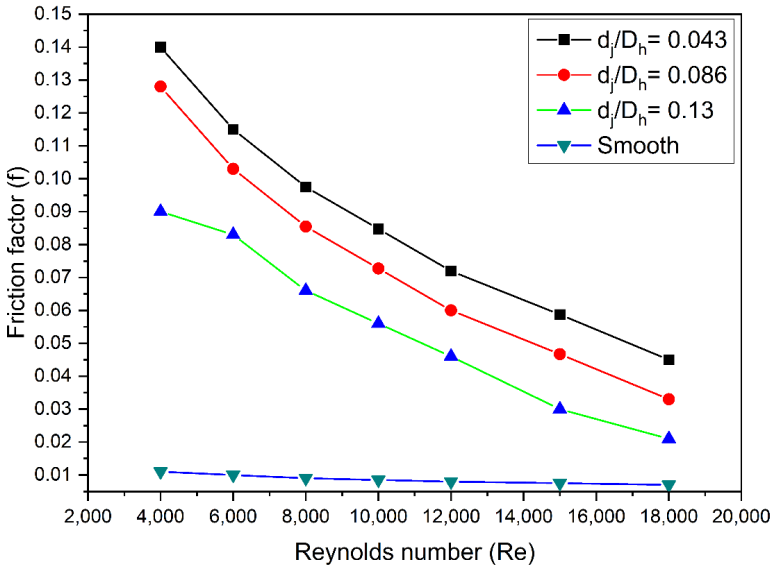

Figure 9. f variation with Re as a function of d_j/D_h.

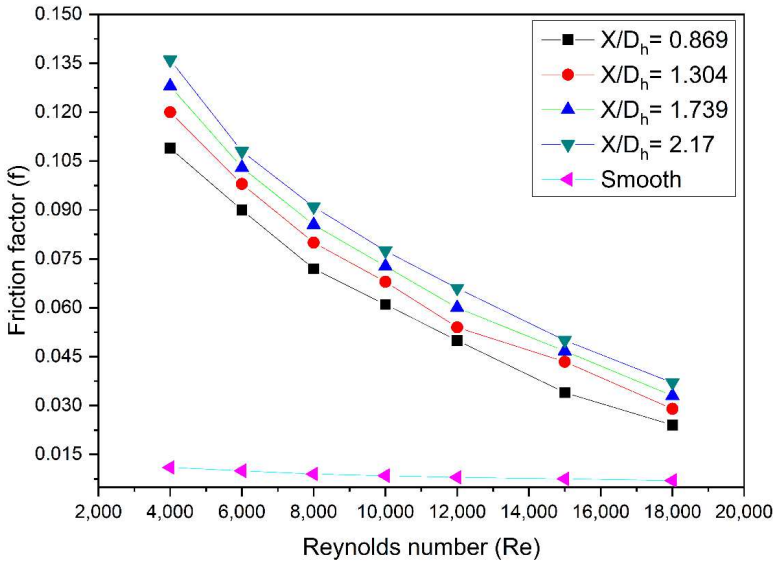

Figure 10. f variation with Re as a function of X/D_h.

The thermo-hydraulic performance parameter (η) is a standard parameter that determines the thermal and friction performance of heat **a** transferring surface, as described by Han et al. [26] and Webb and Eckert [27]. The thermo-hydraulic performance parameter (η) is given as:

$$\eta = \frac{Nu}{Nu_s} / \left(\frac{f}{f_s}\right)^{\frac{1}{3}} \tag{20}$$

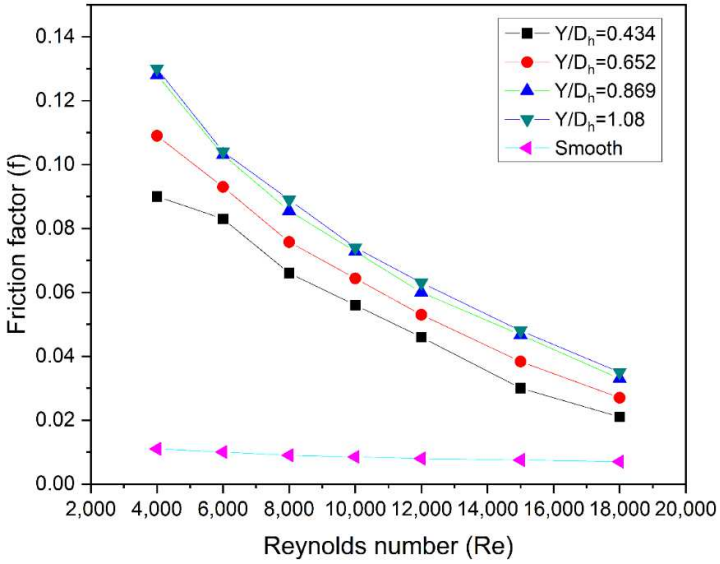

Figure 11. f variation with Re as a function of Y/D_h.

The η determined for the d_j/D_h, X/D_h and Y/D_h parameters are presented in Figure 12 for a range of Re values. It can be seen from Figure 12a that the highest value in terms of η is found at a $d_j/D_h = 0.086$, and the physics behind this is that at $d_j/D_h = 0.043$, the diameter that provides a higher pressure drop penalty is small, and at $d_j/D_h = 0.13$, a larger diameter with a lower turbulent intensity produces a small Nu. Similarly, the effect of X/D_h and Y/D_h on η is presented in Figure 12b,c. The maximum η is achieved at parameters values for X/D_h and Y/D_h of 1.739 and 0.869, respectively. The best η considering the entire set of geometrical parameters was found to be 3.18 at an Re of 15,000, and the staggered pattern also plays a major role in enhancing the heat transfer.

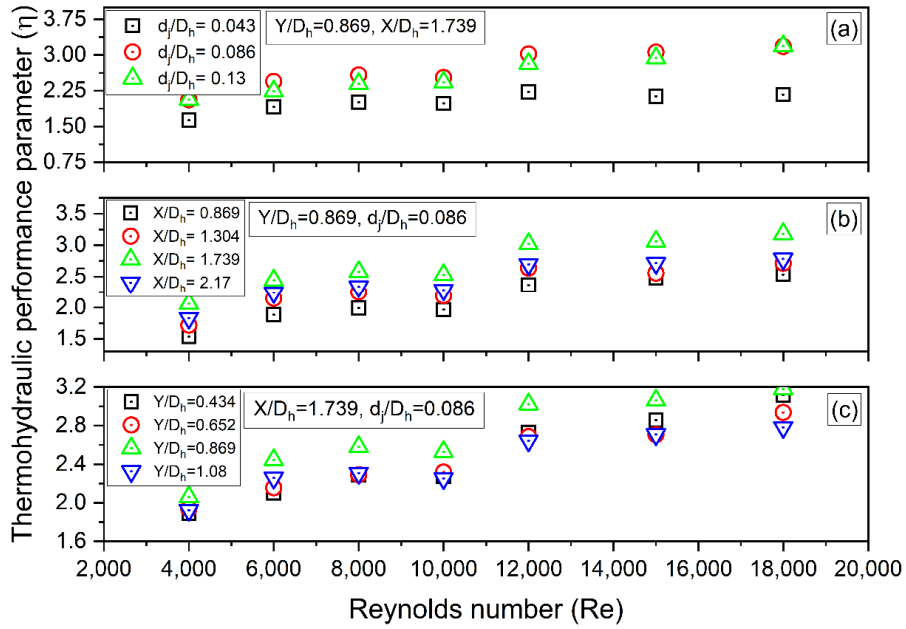

Figure 12. η variation with Re as a function of (**a**) d_j/D_h, (**b**) X/D_h and (**c**) Y/D_h.

The use of impinging jets on the heated surface leads to a higher heat transfer, and augmentation is seen to be further enhanced by the use of roughness on the heated surface. A comparative analysis was carried out on the basis of the thermohydraulic performance of the previously investigated heated surfaces with air jet impinging on them. The compar-

ative graph plotted in Figure 13 represents the present investigation results and the results of various investigations.

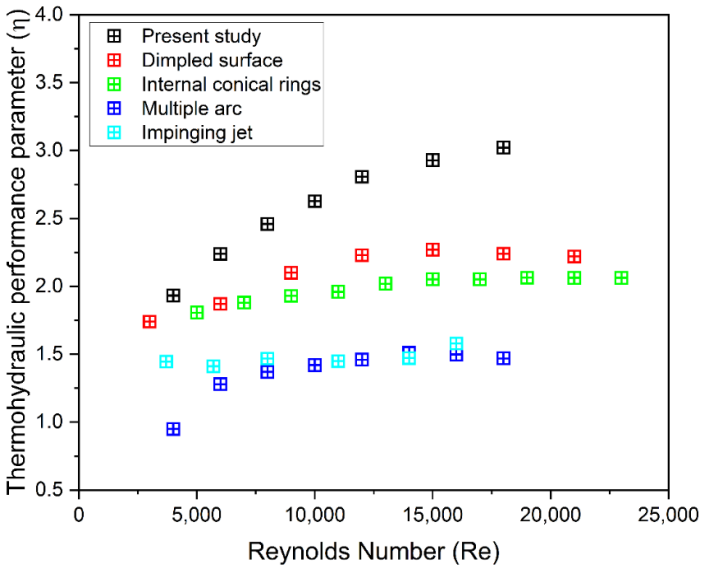

Figure 13. Comparison of η for present and various geometries investigated.

7. Development of Correlations

The extensive experimentation yielded data in dimensionless terms for the Nusselt number (Nu), friction factor (f) and thermohydraulic performance parameter (η) for the selected operating and geometric parameters. The data acquired for the Nu, f and η was observed to be a strong function of the geometric and operating parameters Re, X/D_h, Y/D_h, d_j/D_h.

The data obtained was used to develop the correlation of Nu, f and η by regression analysis to bring about an efficient way of calculating the Nu, f and η data for the selected range of parameters by researchers in future. The regression analysis of the data resulted in the correlation for Nu being:

$$Nu = 0.114 \times Re^{0.94} Pr^{0.4} \left(\frac{X}{D_h}\right)^{0.303} \left(\frac{Y}{D_h}\right)^{0.2} \left(\frac{d_j}{D_h}\right)^{0.71} \quad (21)$$

Correspondingly, the correlation for f developed is written as

$$f = 102.5 \times Re^{-0.89} \left(\frac{X}{D_h}\right)^{0.27} \left(\frac{Y}{D_h}\right)^{0.32} \left(\frac{d_j}{D_h}\right)^{-0.31} \quad (22)$$

$$\eta = 0.96 \times Re^{0.297} \left(\frac{X}{D_h}\right)^{0.21} \left(\frac{Y}{D_h}\right)^{0.24} \left(\frac{d_j}{D_h}\right)^{-0.14} \quad (23)$$

Figure 14a–c displays the deviation in the predicted and experimental values for Nu, f and η, and the deviation was found to be ±11%, ±12%, and ±9%, respectively.

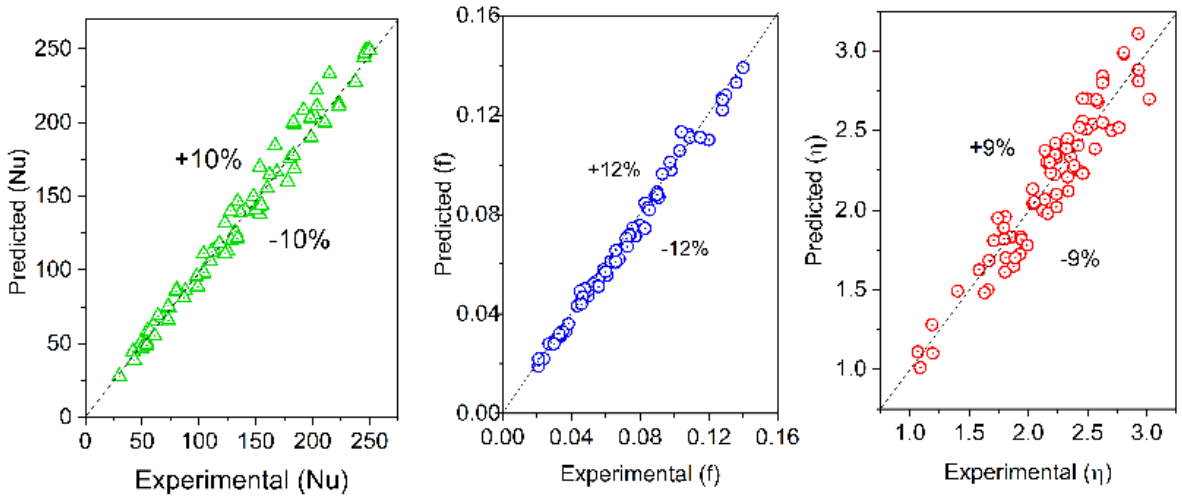

Figure 14. Deviation in predicted and experimental values for (**a**) Nu, (**b**) f and (**c**) η.

8. Exergetic Performance

The energetic performance of a staggered impinging jet on an STC rectangular duct was evaluated in terms of the temperature of the absorber plate, which is a major parameter for measuring performance. It is evident that when the Re increases, there is a higher degree of turbulence intensity, and this leads to the breakdown of the boundary layer formed in the vicinity of the heated surface. This disruption in the boundary layer increases the heat transfer rate from the heated surface to the air, and thus the absorber plate temperature (T_p) decreases. The lower plate temperature reveals that the convective heat transfer coefficient is higher in the case of air jet impinging on a plate, with method resulting in a higher heat transfer coefficient compared to heat transfer without jet impingement on a smooth plate. Values of 0.869, 1.739 and 1.5 for the investigated geometric parameters Y/D_h, X/D_h and d_j/D_h, respectively, yields a minimum plate temperature in terms of the STC duct. The extraction of thermal energy from the heated surface is accompanied by number of exergy losses in the form of heat transfer loss ($EX_{L,HT.}$), optical exergy loss ($EX_{L,Opt.}$), irradiation loss (($EX_{L,Irr.}$), friction loss ($EX_{L,Fri.}$) and fluid heat transfer loss ($EX_{L,FHT}$). The selected geometrical parameters values that deliver the highest Nu results in the exergy losses encountered in Figure 15. An analysis of the plot reveals that the impact of Re on the optical exergy loss ($EX_{L,Opt.}$) is not prominent. The optical exergy loss ($EX_{L,Opt.}$) is the incident radiation reflected back into the atmosphere from the glass cover. Likewise, it is seen that the other exergy losses follow an asymptotic curve, and these exergy losses does not have a dependency on Re. A computation of the total exergy inlet to the system (EX_{IN}), total exergy losses ($EX_{T,Loss}$) and the exergy efficiency (EX_{η}) was carried out and the plot is shown in Figure 16. The plot reveals a maximum exergetic efficiency of 3.87 at a set of geometrical parameters values for Y/D_h, X/D_h and d_j/D_h and an Re of 4000.

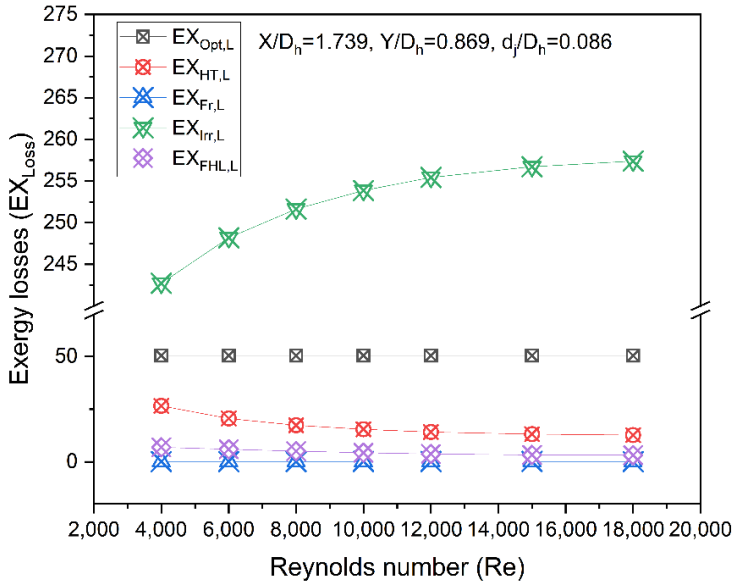

Figure 15. Various exergy losses encountered for varying *Re* values.

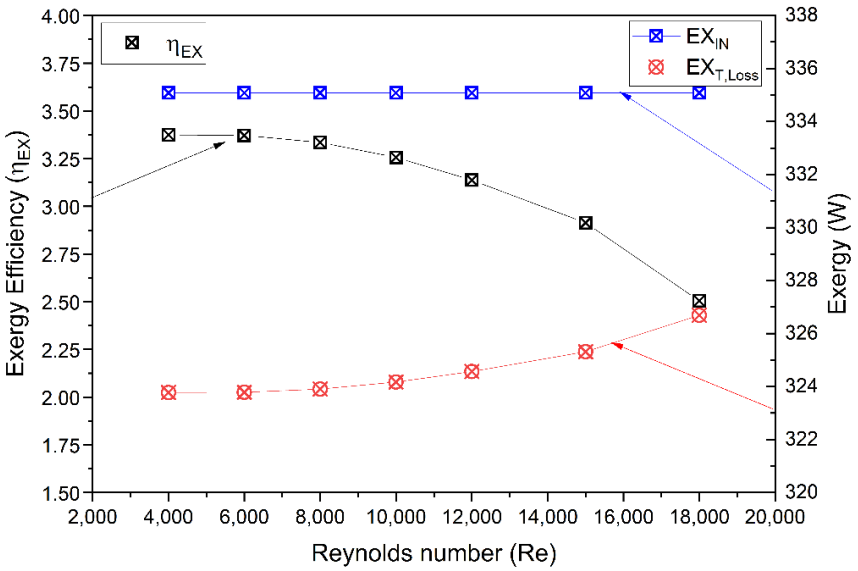

Figure 16. Total exergy inlet, exergy losses and the exergy efficiency for varying *Re* values.

9. Sustainability Index

The sustainability index (SI), waste energy ratio (WER) and improvement potential (IP) are the suggestive parameters for evaluating exergy losses and corresponding irreversibility in thermal systems [28–30]. These three variables are based on an exergy study that ensures long-term viability. The WER and IP increase with an increment in exergy losses, in which case, correspondingly, the SI decreases. The higher the exergy losses, the higher the improvement potential and waste heat that needs to be recovered. These three components are mathematically expressed as:

Sustainability index:

$$SI = \frac{1}{(1 - \eta_{EX})} \tag{24}$$

Waste energy ratio:

$$WER = EX_{T,Loss} / EX_{IN} \tag{25}$$

Improvement potential (W)

$$IP = (1 - \eta_{EX})(EX_{out}) \quad (26)$$

The results for the SI, WER and IP were calculated for all the studied parameters and are represented in Figures 17–19. The SI results imply the life time of the system and WER describes the exergy loss per unit exergy inlet. The SI variation as a function of Re for different values in terms of relative streamwise pitch (X/D_h) are shown in Figure 17a, while the relative spanwise pitch (Y/D_h) and relative jet diameter to hydraulic diameter ratio (d_j/D_h) are kept constant. The SI values vary between 1.0171–1.0347. A higher SI value signifies a higher exergy efficiency and, hence, the system is sustainable on these parameters. An $X/D_h = 1.739$, its optimum value, results in the highest SI. Beyond this (X/D_h) value, the SI decreases because of a higher pressure drop and lower levels of heat transfer. Similar trends were observed when the (Y/D_h) and (d_j/D_h) varied, as can be seen from Figure 17b,c, respectively. The range in terms of SI was 1.0219–1.0349 when the (Y/D_h) varied from 0.434–1.08. Analogous to previous results, the SI variation was 1.0218–1.0349 for a variation in (d_j/D_h) from 0.043 to 0.13.

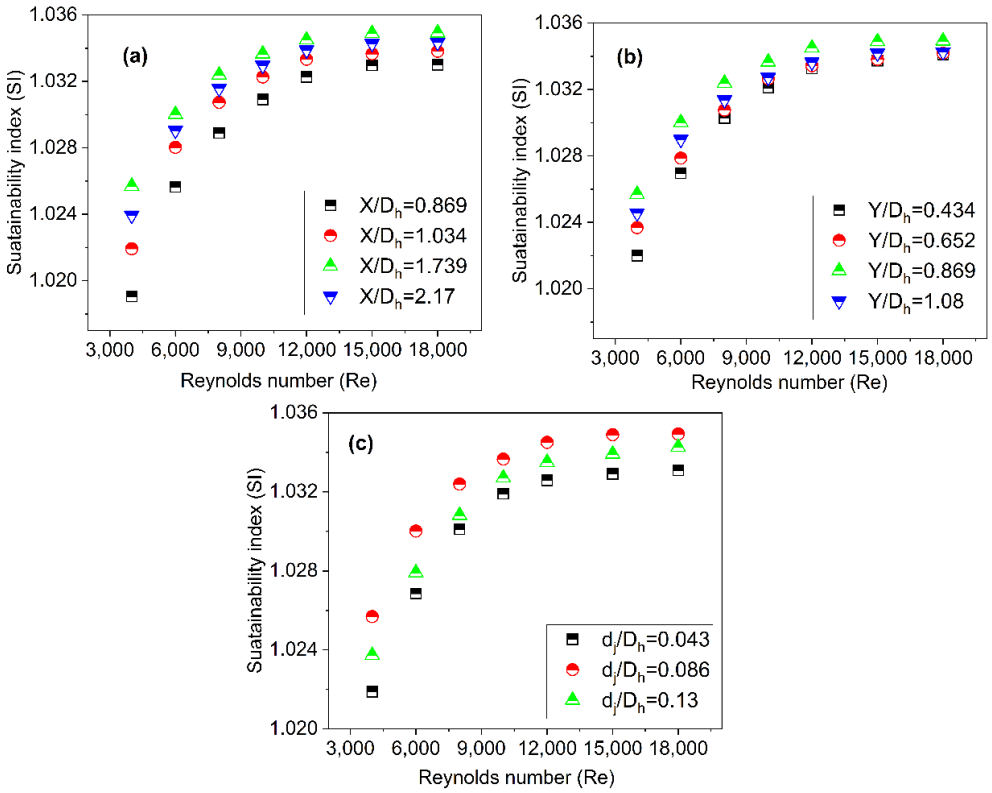

Figure 17. Effect of (**a**) X/D_h, (**b**) Y/D_h and (**c**) d_j/D_h on SI.

The waste energy ratio (WER) represents the exergy loss per unit of exergy available at an inlet. The exergy loss decreases significantly with an increase in the Reynolds number. The decrement in exergy loss signifies that the energy available at the inlet is used for the heating process. As the usage of exergy increases, the WER values decrease, as can be seen in the Figure 18. The WER varies between 0.9665–0.9832, 0.962–0.9832 and 0.97–0.9832 according to varying (X/D_h), (Y/D_h) and (d_j/D_h) values, respectively. At higher values in terms of Re, a higher heat transfer is received and, hence, the lower the WER. Figure 18a, represents the variation in WER as a function of Re by varying the X/D_h from 0.869 to 2.17. The lowest WER value was obtained at an $X/D_h = 1.739$, and the maximum at an X/D_h = 0.869. These trends signify that, among the studied parameters, the exergy losses reach a maximum at lower X/D_h value and a minimum at higher values until the X/D_h

reaches 1.739. Beyond an X/D_h = 1.739 and for all Re values, the WER was higher. The apparent reason for this is that at an X/D_h = 2.17, the heat transfer decreases and, hence, the WER increases. Similar trends in terms of WER variations can be seen in Figure 18b, where (X/D_h) and (d_j/D_h) are kept constant and the WER results as function of Re by varying the (Y/D_h) are shown. The results testify that the optimum Y/D_h value is 0.869, where the WER is at a minimum. The results in terms of WER by varying the (d_j/D_h) are shown in Figure 18c, which shows that a d_j/D_h = 0.086 results in a minimum WER.

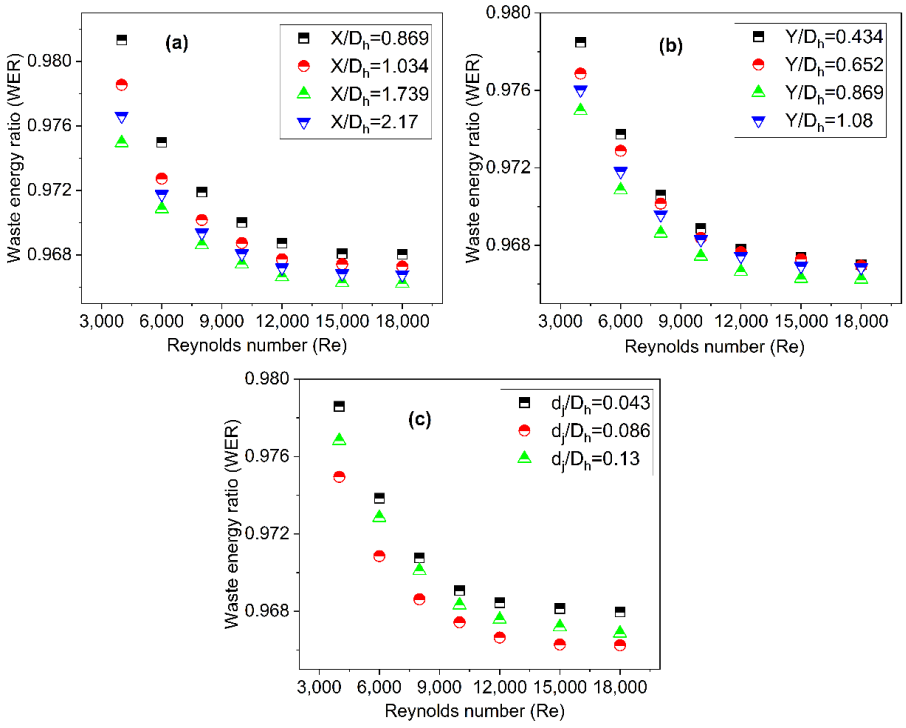

Figure 18. Waste heat recovery (WER) variation for (**a**) X/D_h, (**b**) Y/D_h and (**c**) d_j/D_h.

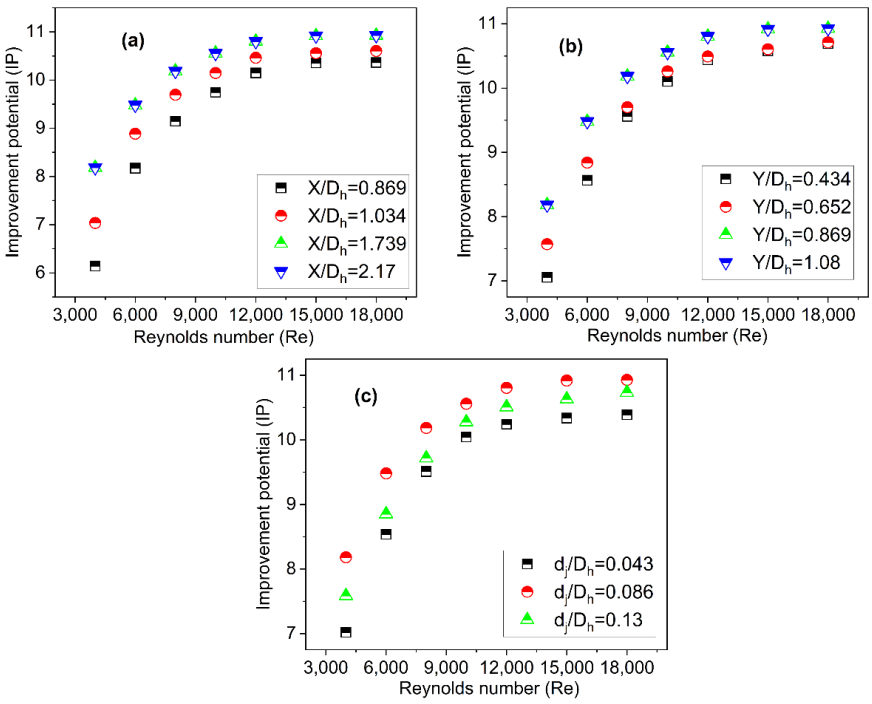

Figure 19. Improvement potential (IP) variation for (**a**) X/D_h, (**b**) Y/D_h and (**c**) d_j/D_h.

In the preceding section, the findings in terms of SI and WER variations with geometric and operational parameters were reviewed. The preceding explanation suggests that the system consumption can be sustained even if exergy losses occur during system operation within the stated range. The third parameter employed in this study was improvement potential (IP), which is used to demonstrate the maximum improvement in the exergy efficiency of the process. The results on IP as a function of Re by varying (X/D_h), (Y/D_h) and (d_j/D_h) values are appended in Figure 19a–c. The results signify that the maximum improvement of the system can be achieved by considering an X/D_h = 1.739 and corresponding parameter values of Y/D_h = 0.869 and d_j/D_h = 0.086. The apparent reason for this is that at these values the exergy losses are at a minimum and the exergy efficiency is at its maximum, which ultimately results in a maximal improvement in system processes. The IP range lies between 2.69–10.84 W. Figure 19a shows the variation in terms of IP at different X/D_h values. The maximum improvement in system performance achieved was 10.84 W at an X/D_h =1.739, while the minimum vape in terms of IP was 5.52 W at an X/D_h = 0.869. The range in terms of IP lies between 6.56–10.84 W for a variation in Y/D_h from 0.434 to 1.08 while X/D_h and d_j/D_h are kept constant, as shown in Figure 19b. The IP results when varying the d_j/D_h and Re are shown in Figure 19c, which shows the range in terms of IP as 6.65–10.84 W.

10. Discussion on Cost Analysis

A CTBR for both a smooth surface and a sine wave-roughened surface solar air heater was computed, and the results are shown in Figure 20. Both heaters would be active for 8 h each day for 300 days, with solar insolation values of 1000 W/m^2. The collector's life expectancy was estimated to be ten years, with a ten percent yearly interest rate. Table 1 shows the costs associated with smooth and roughened air heaters.

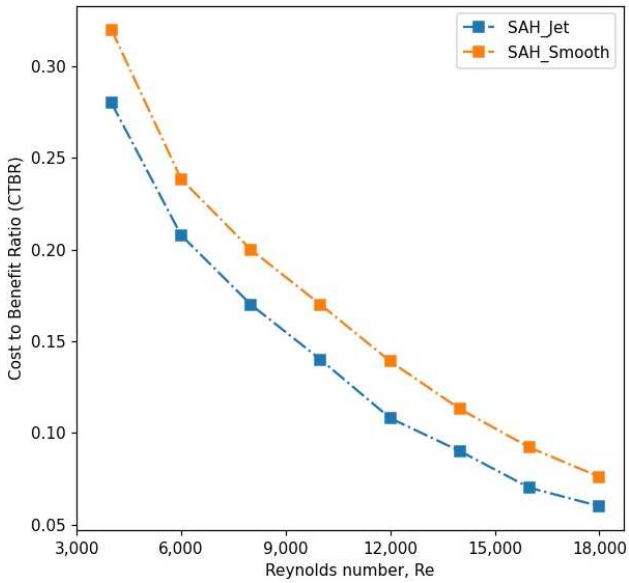

Figure 20. $CBTR$ variations for jet and smooth surface collector.

Table 1. Associated costs.

S.No	Cost Head	For Smooth	For Roughened
1	CCA	\$90/m^2	\$90/m^2
2	SFC	\$85/m^2	\$85/m^2
3	TFC	\$90/m^2	\$100/m^2
4	EC	\$0.065/kWH	\$0.065/kWH

The $CTBR$ value falls when the Re grows from 4000 to 18,000, as seen in Figure 20. The plot reveals that the solar air heater roughened with sine wave baffles is more cost

effective than the smooth surface solar air heater across the evaluated range of geometric and operational parameters.

11. Conclusions

An analysis of staggered impinging jets on staggered spherical protrusions was carried out experimentally with the aim of determining the SI, WER, IP and $CTBR$ from the data generated. The pitches in the stream wise (X/D_h) and spanwise direction (Y/D_h), as well as the jet diameter (d_j/D_h), play an important role in the augmentation of heat transfer, and the staggered arrangement of the jets and protrusion further boost up the turbulence intensity that is responsible for a higher Nu. The following conclusion can be drawn out from the present investigation:

1. The staggering of the impinging jet as well as the spherical protrusion is an effective technique for enhancing thermal performance.
2. The maximum thermohydraulic performance in the present study was achieved at the following parameter values: an X/D_h of 1.739, a Y/D_h of 0.869 and a d_j/D_h of 0.086, for the entire range of Re values selected.
3. The correlations for Nu, f and η were developed and exergy analysis was carried out to reveal a maximum EX_η of 3.87%.
4. The sustainability index (SI), waste energy ratio (WER) and improvement potential (IP) are determined by the exergy losses and corresponding irreversibility. The magnitude of SI, WER and IP determined were 1.034, 0.98 and 10.85, respectively, by determining the exergy losses and corresponding irreversibility.
5. The $CTBR$ of the present jet impingement system was found to be lower than a smooth duct, hence the jet impingement system is more cost effective than the smooth one over the entire range of Re values.

Author Contributions: R.M.—Conceptualization, supervision; A.K.—Methodology, Investigations; M.K.—Methodology, S.S.—Experimentation, Original Draft. All authors have read and agreed to the published version of the manuscript.

Funding: This study received no external funding.

Institutional Review Board Statement: Did not require ethical approval.

Informed Consent Statement: Not applicable.

Data Availability Statement: This study did not report any data.

Conflicts of Interest: The authors declare no conflict of interest.

Nomenclature

$CTBR$	Cost to benefit ratio	T_i	Inlet temperature
AC	Annual costs	V	Velocity of air
EGA	Energy gained annually	X	Streamwise pitch
C_p	Specific heat	Y	Spanwise pitch
d_j	Diameter of jet	$\dot{m}_a$	Mass flow rate of air
ΔP_d	Pressure drop across the duct	Greek letters	
D_h	Hydraulic diameter	ρ_a	Density of air
EX_{out}	Exergy out	υ_a	Kinematic viscosity of air
K	Conductivity of air	η	Thermohydraulic performance parameter
Pr	Prandtl number		
T_o	Outlet temperature		

References

1. Goswami, D.; Vijayaraghavan, S.; Lu, S.; Tamm, G. New and emerging developments in solar energy. *Sol. Energy* **2004**, *76*, 33–43. [CrossRef]
2. Alam, T.; Saini, R.; Saini, J. Use of turbulators for heat transfer augmentation in an air duct—A review. *Renew. Energy* **2014**, *62*, 689–715. [CrossRef]
3. Goel, A.K.; Singh, S.N. Performance studies of a jet plate solar air heater with longitudinal fins. *Int. J. Ambient Energy* **2017**, *40*, 119–127. [CrossRef]
4. Aboghrara, A.M.; Baharudin, B.; Alghoul, M.; Adam, N.M.; Hairuddin, A.A.; Hasan, H.A. Performance analysis of solar air heater with jet impingement on corrugated absorber plate. *Case Stud. Therm. Eng.* **2017**, *10*, 111–120. [CrossRef]
5. Röger, M.; Buck, R.; Müller-Steinhagen, H. Numerical and Experimental Investigation of a Multiple Air Jet Cooling System for Application in a Solar Thermal Receiver. *J. Heat Transf.* **2005**, *127*, 863–876. [CrossRef]
6. Nadda, R.; Kumar, A.; Maithani, R.; Kumar, R. Investigation of thermal and hydrodynamic performance of impingement jets solar air passage with protrusion with combination arc obstacle on the heated plate. *Exp. Heat Transf.* **2017**, *31*, 232–250. [CrossRef]
7. Kercher, D.M.; Tabakoff, W. Heat Transfer by a Square Array of Round Air Jets Impinging Perpendicular to a Flat Surface Including the Effect of Spent Air. *J. Eng. Power* **1970**, *92*, 73–82. [CrossRef]
8. Nadda, R.; Kumar, R.; Kumar, A.; Maithani, R. Optimization of single arc protrusion ribs parameters in solar air heater with impinging air jets based upon PSI approach. *Therm. Sci. Eng. Prog.* **2018**, *7*, 146–154. [CrossRef]
9. Metzger, D.E.; Florschuetz, L.W.; Takeuchi, D.I.; Behee, R.D.; Berry, R.A. Heat Transfer Characteristics for Inline and Staggered Arrays of Circular Jets with Crossflow of Spent Air. *J. Heat Transf.* **1979**, *101*, 526–531. [CrossRef]
10. Chauhan, R.; Thakur, N. Heat transfer and friction factor correlations for impinging jet solar air heater. *Exp. Therm. Fluid Sci.* **2013**, *44*, 760–767. [CrossRef]
11. Brevet, P.; Dejeu, C.; Dorignac, E.; Jolly, M.; Vullierme, J. Heat transfer to a row of impinging jets in consideration of optimization. *Int. J. Heat Mass Transf.* **2002**, *45*, 4191–4200. [CrossRef]
12. Nadda, R.; Maithani, R.; Kumar, A. Effect of multiple arc protrusion ribs on heat transfer and fluid flow of a circular-jet impingement solar air passage. *Chem. Eng. Process. Process Intensif.* **2017**, *120*, 114–133. [CrossRef]
13. Mishra, P.K.; Nadda, R.; Kumar, R.; Rana, A.; Sethi, M.; Ekileski, A. Optimization of multiple arcs protrusion obstacle parameters using AHP-TOPSIS approach in an impingement jet solar air passage. *Heat Mass Transf.* **2018**, *54*, 3797–3808. [CrossRef]
14. Sedighi, E.; Mazloom, A.; Hakkaki-Fard, A. Uniform Cooling of a Flat Surface by an Optimized Array of Turbulent Impinging Air Jets. *Heat Transf. Eng.* **2018**, *40*, 1750–1761. [CrossRef]
15. Afroz, F.; Sharif, M.A. Numerical investigation of heat transfer from a plane surface due to turbulent annular swirling jet impingement. *Int. J. Therm. Sci.* **2020**, *151*, 106257. [CrossRef]
16. Issac, J.; Singh, D.; Kango, S. Experimental and numerical investigation of heat transfer characteristics of jet impingement on a flat plate. *Heat Mass Transf.* **2019**, *56*, 531–546. [CrossRef]
17. Celik, N. Effects of dimples' arrangement style of rough surface and jet geometry on impinging jet heat transfer. *Heat Mass Transf.* **2019**, *56*, 339–354. [CrossRef]
18. Singh, S.; Chaurasiya, S.K.; Negi, B.S.; Chander, S.; Nemś, M.; Negi, S. Utilizing circular jet impingement to enhance thermal performance of solar air heater. *Renew. Energy* **2020**, *154*, 1327–1345. [CrossRef]
19. Kumar, N.; Kumar, A.; Maithani, R.; Thakur, R.; Kumar, R.; Thakur, A. Effect of circular inside conical ring obstacles on heat transfer and friction characteristics of round jets impingement solar air rectangular passage. *Int. J. Green Energy* **2019**, *16*, 1091–1104. [CrossRef]
20. Kumar, N.; Kumar, A.; Maithani, R. Development of new correlations for heat transfer and pressure loss due to internal conical ring obstacles in an impinging jet solar air heater passage. *Therm. Sci. Eng. Prog.* **2020**, *17*, 100493. [CrossRef]
21. Erasmus, D.J.; Lubkoll, M.; von Backström, T.W. Jet impingement heat transfer within a hemisphere. *Heat Mass Transf.* **2020**, *57*, 931–948. [CrossRef]
22. ASHRAE. *Standards, Methods of Testing to Determine the Thermal Performance of Solar Collectors*; ASHRAE: New York, NY, USA, 1977.
23. Klein, S. Calculation of flat-plate collector loss coefficients. *Sol. Energy* **1975**, *17*, 79–80. [CrossRef]
24. Salman, M.; Chauhan, R.; Kim, S.C. Exergy analysis of solar heat collector with air jet impingement on dimple-shape-roughened absorber surface. *Renew. Energy* **2021**, *179*, 918–928. [CrossRef]
25. Fudholi, A.; Sopian, K.; Ruslan, M.H.; Othman, M.Y. Performance and cost benefits analysis of double-pass solar collector with and without fins. *Energy Convers. Manag.* **2013**, *76*, 8–19. [CrossRef]
26. Han, J.; Ou, S.; Park, J.; Lei, C. Augmented heat transfer in rectangular channels of narrow aspect ratios with rib turbulators. *Int. J. Heat Mass Transf.* **1989**, *32*, 1619–1630. [CrossRef]
27. Webb, R.; Eckert, E. Application of rough surfaces to heat exchanger design. *Int. J. Heat Mass Transf.* **1972**, *15*, 1647–1658. [CrossRef]
28. Afshari, F.; Do, A. Energy-exergy and sustainability analysis of a PV-driven quadruple–Flow solar drying system us. *Renew. Energy* **2021**, *175*, 1151–1166.

29. Akpinar, E.K. Drying of mint leaves in a solar dryer and under open sun: Modelling, performance analyses. *Energy Convers. Manag.* **2010**, *51*, 2407–2418. [CrossRef]
30. Nidhul, K.; Yadav, A.K.; Anish, S.; Arunachala, U. Efficient design of an artificially roughened solar air heater with semi-cylindrical side walls: CFD and exergy analysis. *Sol. Energy* **2020**, *207*, 289–304. [CrossRef]